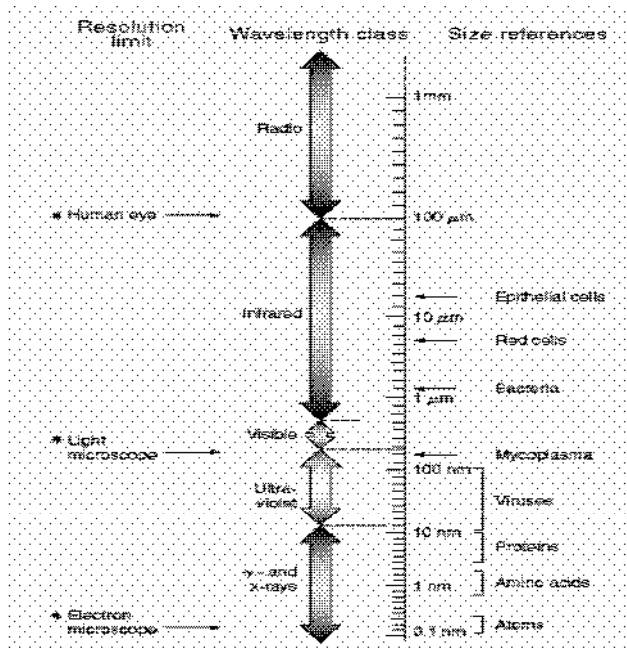# Nonlinear Optics: Applications to Detection and Imaging

Vittorio Degiorgio
Università di Pavia
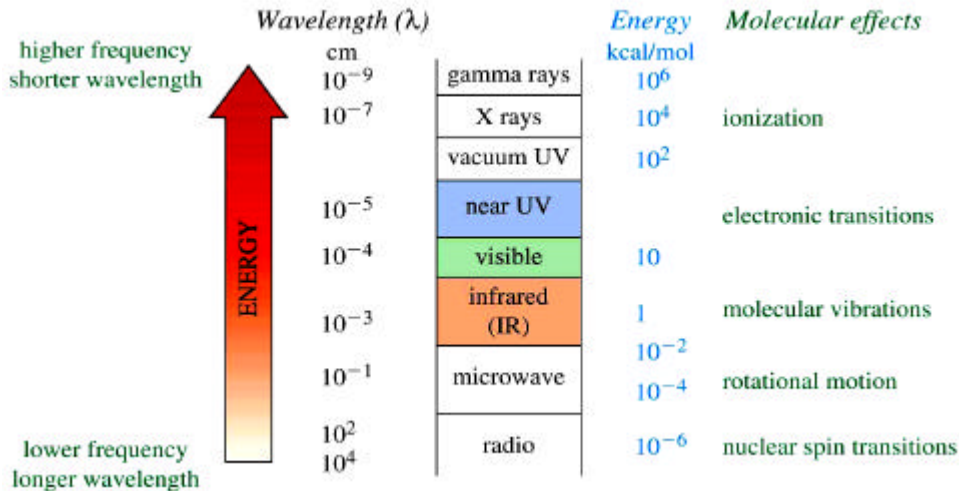
Outline

- Nonlinear optics: general discussion

- Second-order phenomena: second–harmonic generation, parametric effects, nonlinear optical materials

- Third-order phenomena: optical Kerr effect, four-wave mixing, two-photon absorption, stimulated Raman scattering

- Detection: Raman Scattering (SERS, TERS, CARS)

- Imaging: Two-photon microscopy, Third-harmonic generation

Electromagnetic Spectrum

Spectrum and Molecular Effects

Wavelength (λ) cm		Energy kcal/mol	Molecular effects
higher frequency shorter wavelength	10^{-9} gamma rays	10^6	
	10^{-7} X rays	10^4	ionization
	vacuum UV	10^2	
	10^{-5} near UV		electronic transitions
	10^{-4} visible	10	
	10^{-3} infrared (IR)	1	molecular vibrations
	10^{-1} microwave	10^{-2} 10^{-4}	rotational motion
lower frequency longer wavelength	10^2 10^4 radio	10^{-6}	nuclear spin transitions

ENERGY

$E = h\nu$ $\quad$ $\nu = c/\lambda$ $\quad$ ϖ (wave number) $= 1/\lambda$

$1\ eV = 8065.54\ cm^{-1}$
$\quad\quad = 1.24\ \mu m$

Advantages of optical techniques

✓ Non-destructive techniques

✓ Fast with respect to biochemical methods

✓ Real-time measurements

✓ Small quantities needed for measurements

Nonlinear Optics

Maxwell equations plus: $\boldsymbol{D} = e_o\boldsymbol{E} + \boldsymbol{P}$

$$\nabla^2_{\mathbf{E}} - \frac{1}{c^2}\frac{\partial^2_{\mathbf{E}}}{\partial t^2} = \boldsymbol{m}_o\frac{\partial^2_{\mathbf{P}}}{\partial t^2}$$

$$P \approx \varepsilon_o\chi^{(1)}E + \varepsilon_o\chi^{(2)}E^2 + \varepsilon_o\chi^{(3)}E^3 \ldots$$

$\chi^{(2)}$ effects: second harmonic generation, difference- and sum-frequency generation,… (non-centrosymmetric materials)

$\chi^{(3)}$ effects: optical Kerr effect, third-harmonic generation, four wave mixing, two-photon absorption (all materials)

Applications of Nonlinear Optics

- New sources of coherent light:
  - SHG and THG of infrared laser beams
  - optical parametric oscillator
  - Raman laser
  - wave mixing
- Propagation in optical fibers:
  - Solitons
  - Raman amplification
- Devices for optical communications
- Imaging and detection

Origin of nonlinear response
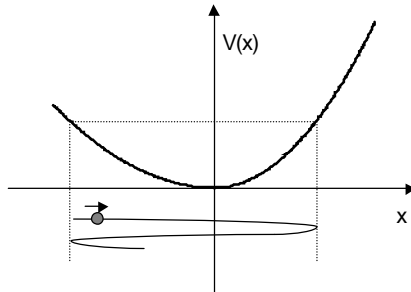
Under the action of the incoming electromagnetic field the bound electron oscillates around its equilibrium position. If the potential well is parabolic (harmonic potential) the oscillation is sinusoidal at the same frequency of the field. If the potential is anharmonic, the oscillation contains higher harmonics. In particular, if the potential contains an antisymmetric term, the oscillation contains the second harmonic term.

Second Harmonic Generation

- Input field: $E_\omega \exp[i(\omega t - k_\omega z)]$

- Nonlinear polarization wave:
  $$P_{NL} = \varepsilon_o \chi^{(2)} E_\omega^2 \exp[2i(\omega t - k_\omega z)]$$

- The nonlinear polarization acts as a source for the second harmonic field at frequency 2ω

SHG: propagation equations

- Assume that the field (real quantity) is given by:
  $E(z,t) = \{E_{\omega}(z)\exp[i(\omega t - k_{\omega}z)] + E_{2\omega}(z)\exp[i(2\omega t - k_{2\omega}z)] + c.c.\}/2$

- Take: $P(z,t) = \varepsilon_o(\chi^{(1)}E + \chi^{(2)}E^2)$

- Substitute into wave equation

- Assume slowly varying amplitudes: $d\,E_{\omega}/dz << k\,E_{\omega}$

- Two equations are obtained by selecting terms oscillating, respectively, at frequency ω and 2ω

SHG: propagation equations

$$\frac{dE_{\mathbf{w}}}{dz} = -i\,\frac{\mathbf{w}}{2n_{\mathbf{w}}c}\,\mathbf{c}^{(2)}E_{\mathbf{w}}^{*}E_{2\mathbf{w}}e^{-i\mathbf{D}kz}$$

$$\frac{dE_{2\mathbf{w}}}{dz} = -i\,\frac{\mathbf{w}}{2n_{2\mathbf{w}}c}\,\mathbf{c}^{(2)}E_{\mathbf{w}}^{2}e^{i\mathbf{D}kz}$$

- Mismatch: $\Delta k = k_{2\omega} - 2k_{\omega}$

- Initial conditions: $E_{\omega}(0) = E_{o}$; $E_{2\omega}(0) = 0$

Phase matching

- Energy conservation:

$$h\omega + h\omega = h2\omega$$

- Momentum conservation:

$$h_{k_\omega} + h_{k_\omega} = h_{k_{2\omega}}$$

Noting that: $k_\omega = (\omega/c)n_\omega$

momentum conservation implies:

$n_\omega = n_{2\omega}$

The velocity of the second harmonic wave should coincide with that of the fundamental wave.

A condition difficult to achieve, because of optical dispersion.

Birefringence phase matching

- Material with negative birefringence:
- Fundamental wave is an ordinary wave, second harmonic wave is an extraordinary wave
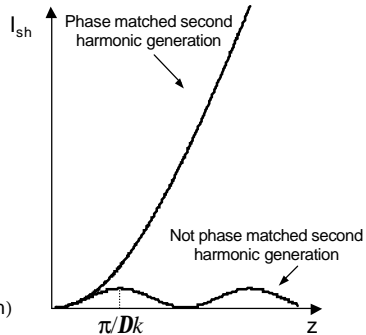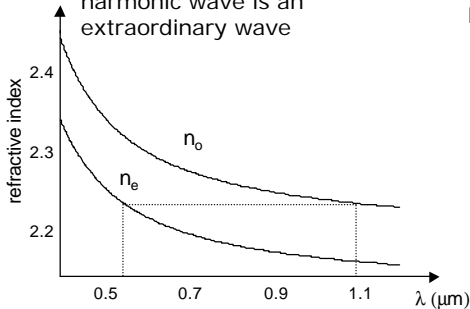
Tuning the phase matching wavelength

Recalling that the index of refraction of the extraordinary wave $n_e(\theta)$ depends on the angle θ between the propagation direction and the optical axis, the phase matching wavelength λ_{pm} can be tuned by changing θ.

Since the indices of refraction depend on temperature, it is also possible to change slightly λ_{pm} by changing the crystal temperature.

$$\frac{1}{n_e^2(\theta)} = \frac{\sin^2 \theta}{n_e^2} + \frac{\cos^2 \theta}{n_o^2}$$

Second Harmonic Generation

- $E_{2\omega}(z) = -i(2n_\omega/n_{2\omega})^{1/2}E_\omega(0)\tanh(z/L_{SH})$

- $I_{2\omega}(z) = I_\omega(z)\tanh^2(z/L_{SH})$

- If $z >> L_{SH}$, there is total conversion! Crystal length at which significant conversion is achieved:

- $$L_{SH} = \lambda/(\chi^{(2)}E_\omega).$$

- Note that, in practical cases, $\chi^{(2)}E_\omega << 1$. If we want L = 1.5 cm = $10^4 \lambda$, and we take $\chi^{(2)} = 10$ pm/V, we find $E_\omega = 10^7$ V/m. This corresponds to a laser intensity:
  $I_w = 10$ MW/cm^2

- Internal field (H atom): 5×10^{11} V/m.

SHG: tensorial notation

-
$$P_i^{2w} = e_o \sum_{j,k=1}^{3} c_{ijk} E_j^w E_k^w$$

- Depending on crystal symmetry, only some of the 27 components of $\chi^{(2)}$ may be different from 0.
- By fixing the propagation direction and the polarization of the incident field, we select specific components of $\chi^{(2)}$.
- Example: we call z the optical axis of the crystal, the incident field propagates along the y-axis and is linearly polarized along x-axis (ordinary wave), the only active components are χ_{111} and χ_{311}. If the field is polarized along the z-axis (extraordinary wave), the only active components are χ_{133} and χ_{333}.

Second-order materials

- Non-centrosymmetric crystals:
- - Inorganic crystals based on oxygen polyedra
- - Heteropolar semiconductors
- - Organic molecular crystals

- Other materials:
- - Polymer matrix containing ordered non-centrosymmetric molecules
- - Poled glasses
- - Asymmetric quantum wells

Second-order materials

- Inorganic crystals based on oxygen polyedra

- - ferroelectric perowskites, $LiNbO_3$ and $KNbO_3$, and $KTiOPO_4$ (KTP): large $\chi^{(2)}$, low damage threshold, transparent in the visible and near infrared (0.35-4.5 μm), phase-matchable by birefringence and by periodic poling, waveguides

- - borates, β-BaB_2O_4 (BBO) and LiB_3O_5 (LBO): medium $\chi^{(2)}$, high damage threshold, transparent in the near UV (0.19-2.5 μm), phase-matchable by birefringence

Second-order materials

- Heteropolar semiconductors: GaAs, CdTe, CdS
- - large $\chi^{(2)}$(40-200 pm/V),
- - difficult phase-matching because birefringence is zero (cubic crystal structure) or very small
- - small energy gap, this means that it is easy to create free carriers (from two-photon absorption or mid-gap impurity states)

Organic materials for nonlinear optics

- Limitations of PPLN and similar inorganic crystals: nonlinearity is not very large, photorefractive effects put a limit to usable pump power
- Organic molecules (from the family of paranitroaniline) possessing very large second-order optical polarizabilities can be designed and synthesized
- In order to have a non-centrosymmetric medium the molecules have to be organized either by growing an **organic crystal** or by dispersing them in a **polymer film** and aligning with an external electric (or optical) field

Periodical poling
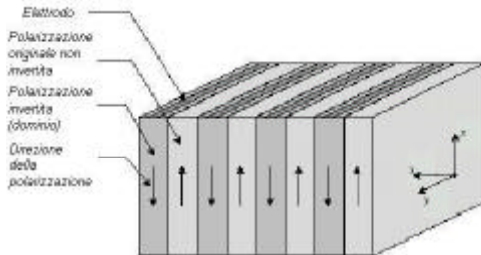
Periodic modulation of the $\chi^{(2)}$ coefficient. In ferroelectric crystals can be obtained by applying strong electric fields

$\chi^{(2)}(z) = \chi_o^{(2)} + \chi_i^{(2)} \exp (2\pi i z/\Lambda)$

Phase matching condition $k(\lambda_{sh}) - 2k(\lambda_p) = 2\pi/\Lambda$

Phase matching @1.55 μm in lithium niobate $\Lambda = 15 \div 18 \ \mu$m

Parametric effects

- If two beams, possessing different frequencies ω_1 and ω_2, and different wave-vectors $\mathbf{k_1}$ and $\mathbf{k_2}$, are sent into a second-order nonlinear crystal, the nonlinear polarization can give rise to new frequencies representing the second-harmonic of each beam or the sum/difference of the input frequencies. By choosing a specific phase-matching condition, only one process is selected among all possible processes. If we select difference-frequency generation (DFG), and assume $\omega_1 > \omega_2$, we obtain a new beam at frequency $\omega_3 = \omega_1 - \omega_2$ and wave vector $\mathbf{k_3}$, provided that the condition: $\mathbf{k_3} = \mathbf{k_1} - \mathbf{k_2}$ is satisfied. In the DFG process, one photon at frequency ω_1 is annihilated and two photons at frequencies, respectively ω_3 and ω_2, are created, so that the process not only produces a new coherent beam at ω_3, but also amplifies the beam at ω_2. Such an amplification process is called parametric amplification.

Parametric effects

- Whereas standard optical amplifiers work only at frequencies corresponding to transitions among energy levels, parametric amplifiers use transparent crystals and can work, in principle, over the whole transparency window of the crystal, provided that phase-matching can be achieved.

- Recalling that an optical amplifier can become a laser oscillator once inserted into an optical cavity, a similar approach can transform the parametric amplifier into a parametric oscillator. Whereas in the laser case the trigger to cavity oscillation comes from spontaneous emission from the upper level of the amplifying medium, the initial seed for parametric oscillation comes from parametric fluorescence, the process by which the "pump" photon at frequency ω_1 spontaneously breaks down into two photons at frequencies ω_2 (signal) and ω_3. (idler).

Parametric oscillator
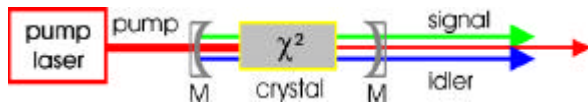
Output of a parametric oscillator
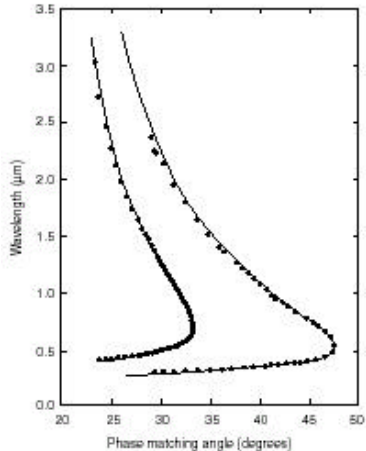
Tuning curves for an optical parametric oscillator pumped by the third- or fourth-harmonic of the Nd-laser frequency. Tuning is performed by rotating the BBO crystal.

Third-order phenomena: optical Kerr effect

$$\frac{dE_w}{dz} = -i\frac{w}{2n_w c}a c^{(3)} E_w^* E_w E_w$$

where a is a numerical constant.

- Initial condition: $E_w(0) = E_o$;
- If $\chi^{(3)}$ is real, the solution is: $E_w(z) = E_o exp[-i(w/c)n_2 Iz]$, where I is the intensity and

$$n_2 = \frac{3 c^{(3)}}{4c e_o n_o}$$

- Kerr effect: the index of refraction becomes
- $\qquad\qquad n = n_o + n_2 I$

Third-order phenomena: two-photon absorption

- If $\chi^{(3)}$ is complex, the propagation equation for the intensity is:

$$\frac{dI}{dz} = -\boldsymbol{b}I^2$$

$$\boldsymbol{b} = \frac{3\boldsymbol{w}}{2\boldsymbol{e}_o c^2 n_o^2} \operatorname{Im}\left\{\boldsymbol{c}^{(3)}\right\}$$

β (in units of *m/W*) is the two-photon absorption coefficient.

- The solution is:

$$I(z) = \frac{I_o}{1 + \boldsymbol{b}zI_o}$$

Third-order phenomena: Four Wave Mixing (FWM)

Two examples of wave mixing in a $\chi^{(3)}$ material.

In the first case, ω_1 is a strong beam, ω_2 is a weak beam, the new frequency ω_3 is generated as: $\omega_3 = 2\omega_1 - \omega_2$.

In the second case, by sending two strong counter-propagating beams 1 and 2 and a weak beam 3, the beam 4 is generated (conjugate mirror)

Light scattering

scattering medium

ω_p

scattered light
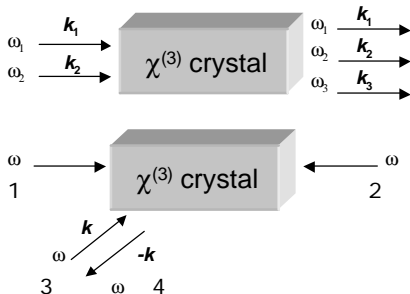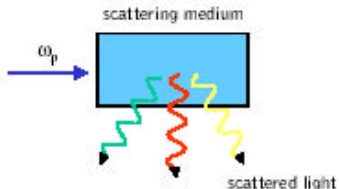
Rayleigh scattering
  scattering from *nonpropagating* density
  fluctuations (elastic)
Brillouin scattering
  scattering from *propagating* presure waves
  (sound waves, acoustic phonons)
Raman scattering
  interaction of light with vibrational modes of
  molecules or lattice vibrations of crystals
  (scattering from optical phonons)

spectrally resolved detection

I_s

Stokes   anti-Stokes

Raman   Rayleigh   Raman
         Brillouin

ω_p ω

Light scattering

V = virtual level

Stokes

anti-Stokes

Rayleigh scattering
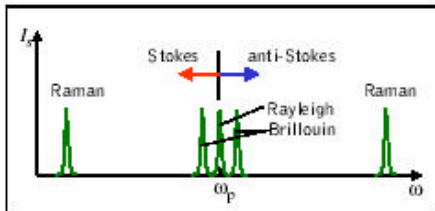
Spontaneous Raman scattering
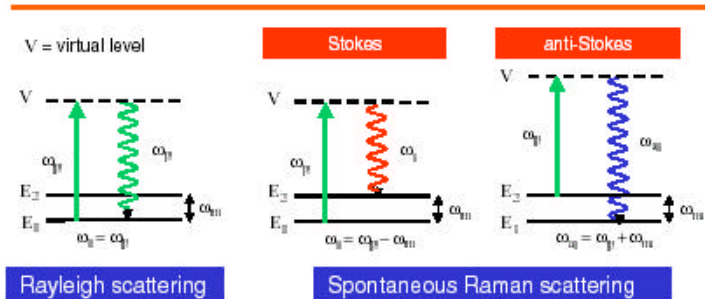
✓ parametric process
✓ scattered photon into arbitrary direction

✓ spontaneous process
✓ scattered photon into arbitrary direction

$$N_2 = N_1 e^{-\hbar\omega_m / kT}$$

⇒ anti-Stokes lines much weaker

Nobel Laureate in 1930

Sir Chandrashekhara Venkata Raman
1888-1970

Raman scattering from proteins
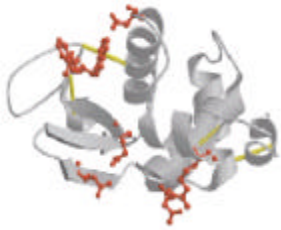
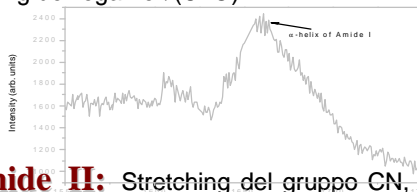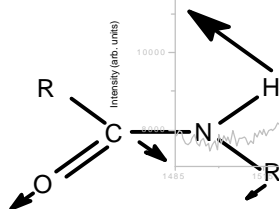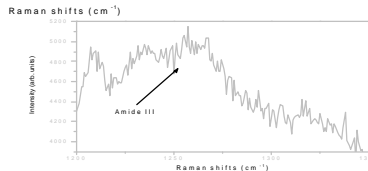**Lisozima**
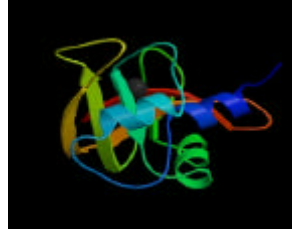
Ribonucleasi-B
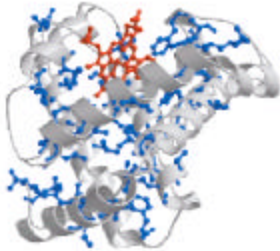
Mioglobina
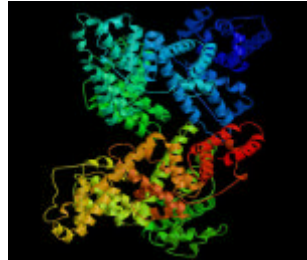
BSA

Strutture delle ammidi e relativi modi vibrazionali
(blocchi elementari presenti nelle proteine)
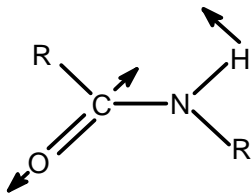
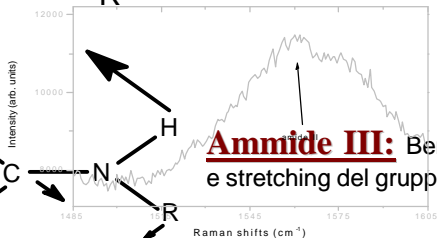**Ammide I:** Il maggiore contributo è apportato dallo stretching del legame $\nu(C=O)$.
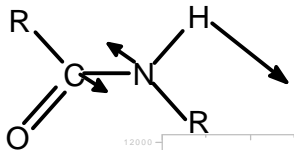
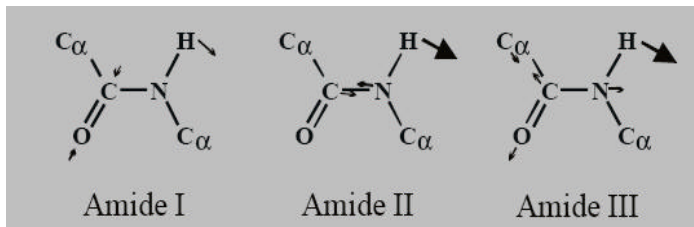**Ammide II:** Stretching del gruppo CN, e bending in piano del gruppo NH.

Ammide III: Bending in piano del gruppo NH ed R e stretching del gruppo CN.

Amides structure & their Raman vibrational modes

Schematic representation of vibrational modes
of Amide I, Amide II, and Amide III

| Raman Markers of Amide I and Amide III in Proteins		
Secondary structure	Amide I (H_2O) cm^{-1}	Amide III (H_2O) cm^{-1}
β-sheet	1665-1680	1230-1240
α-helix	1645-1660	1260-1300
unordered	1660-1665	1240-1250

? Le vibrazioni delle ammidi I, II e III danno origine alle bande più intense e quindi più facili da individuare.

? Le intensità e le frequenze delle bande dovute ai modi vibrazionali dell'ammide dipendono dalla struttura secondaria della proteina in quanto la conformazione proteica dipende dai legami – H tra i vari gruppi ammidici.

? Le frequenze di vibrazioni osservate nelle ammidi I e III in relazione alla conformazione, sono molto utili per determinare il grado di denaturazione di una proteina.

Lisozima
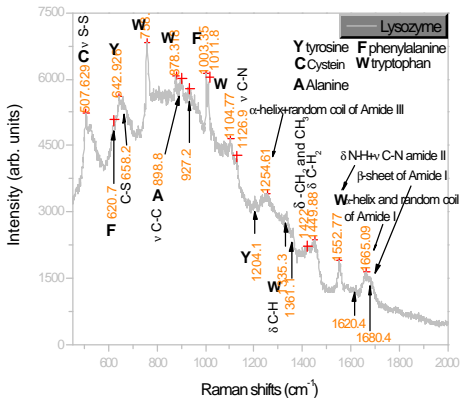
- Struttura secondaria delle ammidi I, II, III.

- La banda dell' ammide II è molto visibile a 1552 cm^{-1}.

- Le bande centrate nel range tra 1630-1690 cm^{-1}, mostrano il contributo dell'a-elica, dei ripiegamenti casuali e del foglietto ß della struttura secondaria.

- Le bande riferite a: Cisteina, Tirosina, Triptofano e Fenilalanina, sono ben visibili.

- L'intensità della banda a 755 cm^{-1} si riferisce all'idrofobicità della proteina.

Mioglobina
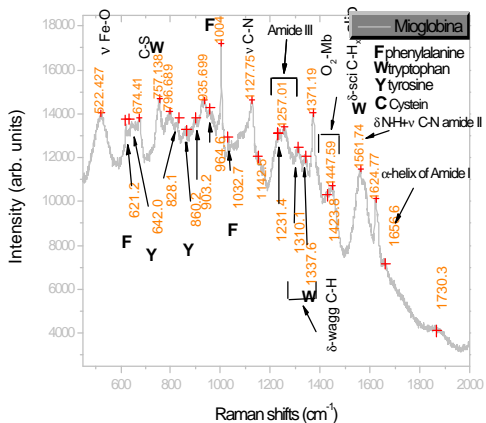
- Notiamo la presenza di Cisteina (522 cm⁻¹), Tirosina (840 cm⁻¹) Triptofano (757 cm⁻¹) e Fenilalanina (1620 cm⁻¹).

- Il picco del gruppo prostetico "eme" si osserva a 522 cm⁻¹.

- Il picco a 1371 cm⁻¹ è relativo al legame che forma la mioglobina con l'ossigeno $\nu(Mb-O_2)$.

- Il picco a 758 cm⁻¹ ci conferma l'idrofobicità della molecola.

- Le ammidi I sono osservate eccezionalmente mentre l'ammide II e III si rilevano con precisione.

Albumina del siero di bovino (BSA)

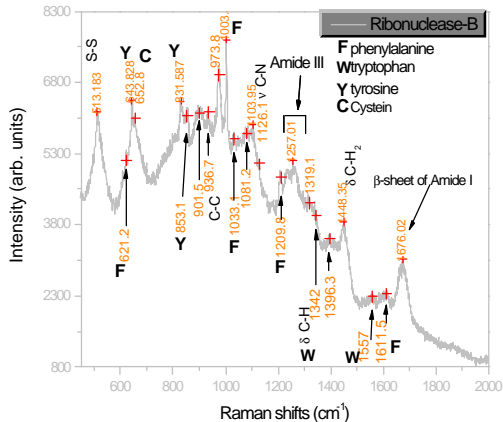- Presenza di Cisteina, Tirosina, Triptofano, e Fenilalanina.
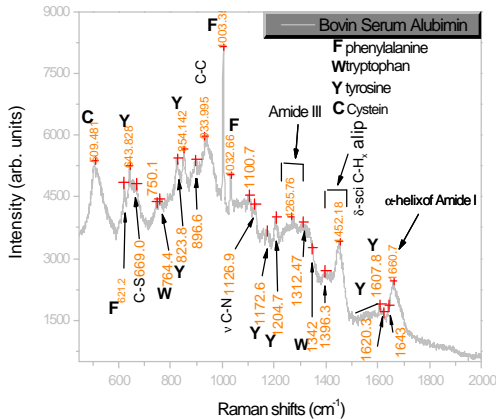
- Sono visibili nello spettro le bande che si riferiscono ai legami: C-C, C-S, N-H e C-H$_x$.

  I ponti S-S sono riscontrati a circa 510 cm^{-1}. Questa banda è fondamentale per determinare la struttura terziaria della proteina.

- Nell'ammide I la presenza della struttura secondaria è più evidente rispetto all'ammide II e III.

- I picchi a 825 e a 855 cm^{-1}, mostrano l'interazione tra l'idrogeno del gruppo –OH della catena laterale della Tirosina e le molecole circostanti.

Ribonucleasi-B

- Presenza significativa di Cisteina, Tirosina, Triptofano e Fenilalanina.

- La banda vibrazionale che ci permette di identificare i ponti disolfuro è osservata a 513 cm⁻¹.

- La minore intensità della banda a 755 cm-1 spiega il comportamento idrofobico.

- Siamo in grado di osservare chiaramente la banda attribuita al foglietto ß dell'ammide I a 1676 cm⁻¹.

- La ribonucleasi notiamo una notevole presenza del foglietto ß, mentre nella BSA troviamo soprattutto a-elica.

Miscela di proteine (Lis.,BSA,Miog.,RNAs-B)
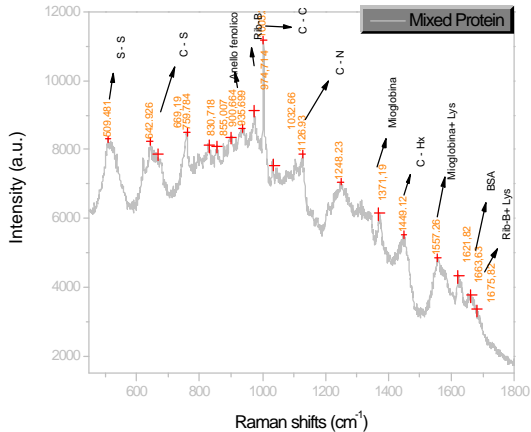
- Le bande ottenute sono il risultato del contributo delle proteine presenti nella miscela.

- La banda a 1663 cm^{-1}, con spalla a circa 1675 cm^{-1}, rappresenta rispettivamente la BSA e il lisozima.

- La banda larga a 1555 cm^{-1} e, la banda stretta a 1371 cm^{-1}, derivano dalla mioglobina con un piccolo contributo del lisozima.

- Il picco acuto a circa 975 cm^{-1} deriva dalla ribonucleasi-B.

- Sono ben visibili i picchi che si riferiscono ai gruppi delle catene alifatiche δ C-H$_x$, ν C-N, C-C, ν C-S e ν S-S.

Surface-enhanced Raman scattering (SERS)

Surface Enhanced Raman Spectroscopy, or Surface Enhanced Raman Scattering, often abbreviated SERS, is a surface sensitive technique that results in the enhancement of Raman scattering by molecules adsorbed on rough metal surfaces. The enhancement factor can be as much as 10^{14}-10^{15}, which allows the technique to be sensitive enough to detect single molecules.

The increase in intensity of the Raman signal for adsorbates on particular surfaces occurs because of an enhancement in the electric field provided by the surface. When the incident light in the experiment strikes the surface, localized surface plasmons are excited. The field enhancement is greatest when the plasmon frequency, $?_p$, is in resonance with the radiation. Furthermore, in order for scattering to occur, the plasmon oscillations must be perpendicular to the surface; if they are in-plane with the surface, no scattering will occur. It is because of this requirement that roughened surfaces or arrangements of nanoparticles are typically employed in SERS experiments as these surfaces provide an area on which these localized collective oscillations can take place. The choice of surface metal is also dictated by the plasmon resonance frequency. Visible and near-infrared radiation (NIR) is used to excite Raman modes. Silver and gold are typical metals for SERS experiments because their plasmon resonance frequencies fall within these wavelength ranges, providing maximal enhancement for visible and NIR light. Copper is another metal whose absorption

spectrum falls within the range acceptable for SERS experiments.

Surface-enhanced Raman scattering (SERS)

The light scattering by metal particles is a two photon process. In the Rayleigh scattering a photon is absorbed by the the metal with the creation, excitation of **surface plasmon modes** and a second photon is emitted with the destruction, annihilation of those modes. Since we are still considering an elastic process the frequency of the emitted photon remains the same as in the incident photon. The others component of the wavevector have changed. When a molecule is adsorbed on the metal surface, the stored energy may be transferred via dipole-dipole interaction to the molecule.

Vibrational modes in the molecule may be activated before having a further energy transfer, this time from the molecule back to the metal. Now, the scattered photon has a different energy and the difference in **energy** should be the quantity gained or lost by the molecule through its vibration. In that sense we may refer to this process as a **surface enhanced Raman scattering (SERS).**

In the normal resonance Raman the molecule interacts directly with the electromagnetic field associated with the traveling wave. In **SERS** this field is already modulated by the electron cloud oscillation in the metal and the molecule experience an enhanced field.

SERS mechanism

Surface Enhanced Raman Spectroscopy (SERS)

I. Electromagnetic effect
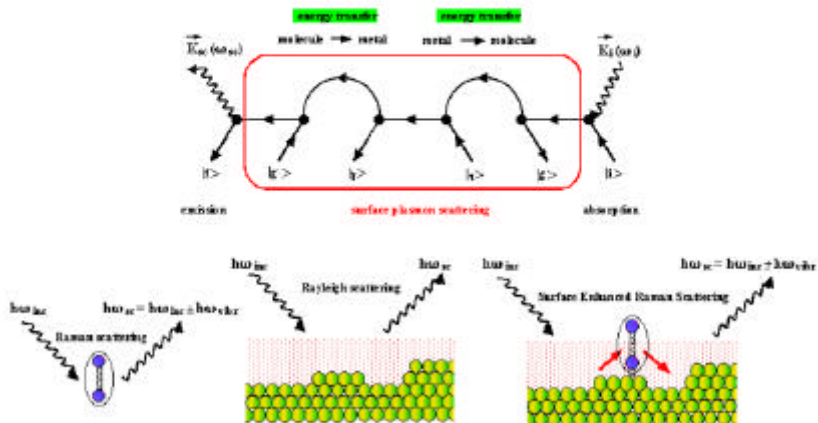
Surface-enhanced Raman scattering (SERS)

Oligonucleotide Targeting SERS can be used to target specific DNA and RNA sequences using a combination of Au and Ag nanoparticles and Raman active dyes (such as Cy3). Specific SNPs (single nucleotide polymorphisms)can be identified using this technique. The gold nanoparticles facilitate the formation of a silver coating on the dye labeled regions of DNA or RNA, allowing SERS to be performed. This has several potential applications: for example Cao et al. report that that gene sequences for HIV, Ebola, Hepatitis, and Bacillus Anthracis can all be uniquely identified using this technique. Each spectrum was specific, which is advantageous over fluorescence detection; some fluorescent markers overlap and interfere with other gene markers. The benefits of using this technique to identify gene sequences is that there is a large amount of commercially available Raman dyes on the market, which could lead to the development of non-overlapping probes for gene detection.
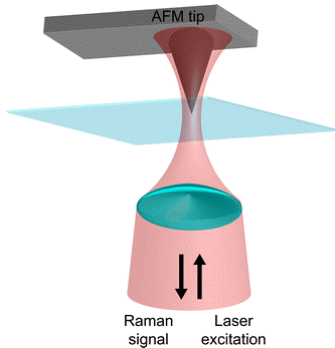
Surface-enhanced Raman scattering (SERS)

After the discovery of surface-enhanced Raman scattering (SERS), a new era started for Raman spectroscopy. SERS research inspired Raman spectroscopy and is still motivating the development of the technique 30 years later.

While the general sensitivity of SERS is not the question, the main obstacle when using SERS for the investigation of interfaces is the inhomogeneity of the SERS substrate across the sample. The different shapes, sizes and roughness of single particles and clusters result in strong variations in the field enhancement and consequently the Raman signal. Furthermore, these physical parameters also depend critically on the substrate preparation. Therefore, a spatially resolved quantitative analysis of interfaces using SERS is impossible.

It is well known that the large field enhancement at metal particles occurs in regions of high curvature and maximum enhancement occurs for elongated particles with dimensions of about 10–100 nm. While clusters are considered to yield a better overall enhancement, a single isolated metal nanoparticle can also enhance the field considerably.

Wessel proposed a scheme to ensure a constant field enhancement using just one single metal nanoparticle for the investigation of a surface. This introduced for the first time the potential of quantitative SERS surface analysis. In this design the rough metal film was replaced by a sharp metal tip that should act as an exclusive active site, which also represents the limit for any SERS experiment—at least one particle is required. The tip should then be scanned over the sample surface using scanning probe microscopy (SPM) techniques. The later experimental verification of this now called *T*ip-*E*nhanced *R*aman *S*cattering (TERS) proved that, in addition to the field enhancement, the lateral resolution of the method was also improved down to 10 nm, due to the small size of the probe.

TERS

The figure shows a schematic diagram of a tip-enhanced Raman scattering setup working in back-reflection mode. An inverted Raman microscope is coupled with an AFM for synchronized use. The microscope is required to illuminate the metal coated AFM tip. The back scattered Raman signal is collected through the same objective and notch or edge filter are used to block the laser line. After this filter stage, the signal is coupled to a spectrometer equipped with a cooled charge-coupled device (CCD)

for spectrally resolved measurements.

TERS
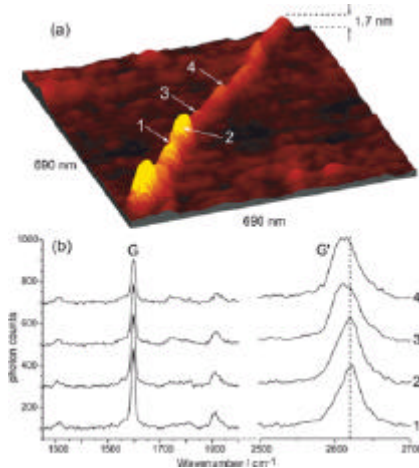
Fig. 12 (a) Three-dimensional topographic image of a single nanotube on glass. (b) Near-field Raman spectra detected at positions 1 to 4 shown in (a). By courtesy of Prof. Dr Achim Hartschuh. A frequency shift in the band position has not been observed for the G band, but significant strong shifts were detected for the G band. The spectral fluctuations represent changes in the SWCNT structure, which can be related to external stress produced by local defects or particles from the catalyst. Such results cannot be provided by any other method and again indicate the potential of the TERS system.

TERS
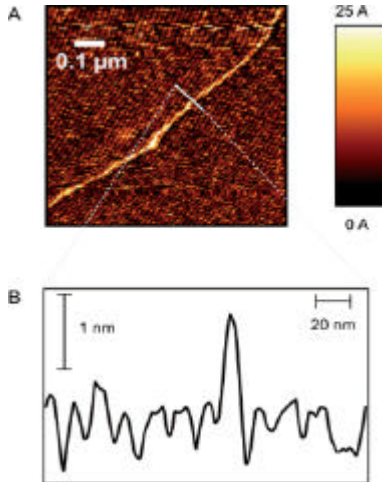
Fig. 13 (A) Topographic image of a cytosine single-stranded RNA homopolymer. (B) Height profile through the RNA at the indicated position.
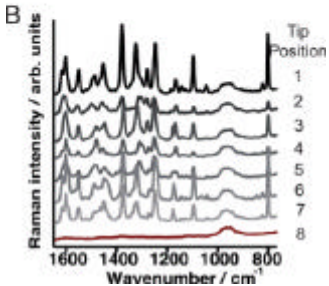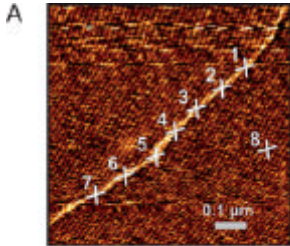
TERS

Fig. 14 TERS experiment along a RNA strand. (A) Topographic image (same as Fig. 13A). (B) TERS spectra at the seven adjacent (1–7) spots correspondingly marked in (A), position 8 marks a reference measurement.

TERS on living cells

Cells (bacteria)

As an example of even more complex samples, TERS studies on living cells are presented. *Staphylococcus epidermidis* is the sample organism used for this TERS experiment. According to the bibliography, the cell surface of *S. epidermidis*, and specifically its cytoplasm membrane, is mainly composed of a peptidoglycan layer, which is pervaded by other polysaccharides and a variety of surface proteins. This is a typical composition of the cytoplasm membrane in all Gram-positive bacteria. It is also likely to find other polysaccharides, *e.g.* teichoic acid or PIA (polysaccharide intercellular adhesion), depending on the growth conditions. Fig. 15 shows the topographic image of *S. epidermidis* cells achieved with an AFM experiment using an ultra sharp silver-coated AFM tip in intermittent mode. The first TER spectra stem from the cell surface—the second spectrum corresponds to a background reference from the glass surface. The enhancement factor was calculated to be around 10^4-10^5. The majority of TERS peaks on the bacteria surface could be tentatively assigned to peptides, lipids and carbohydrates abundant on the cell surface of bacteria. Hence, the TERS experiment provides similar information as previous SERS research on whole cells.

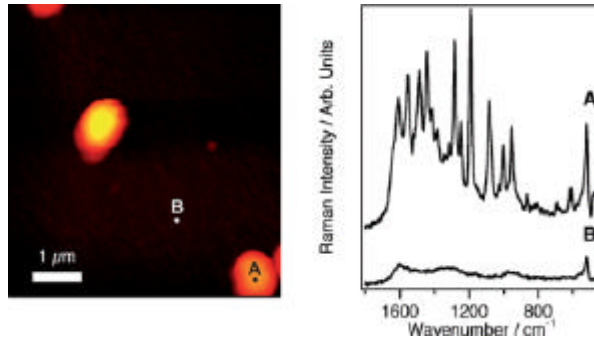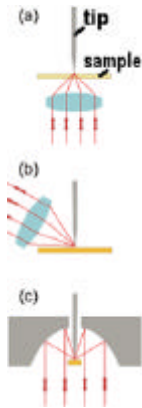# *T*ip-*E*nhanced *R*aman *S*cattering (TERS)

Fig. 15 (a) Topographic image of *S. epidermidis* cells. (b) Tip-enhanced Raman spectra of the marked positions in (a). Position (A) corresponds to a TERS spectrum on the cell surfaces, and position (B) corresponds to a reference TERS experiment on the glass surface.

TERS set-up schemes

The laser beam is focused onto the tip-sample gap via a microscope objective, having 50X or 100X magnification or with a parabolic mirror. In case a) inverse illumination, the substrate must be transparent, in cases b) side illumination with an objective, and c) top illumination with a parabolic mirror, the substrate can be opaque. In all cases backscattering geometry is used. We use a He-Ne laser (632.8 nm) with low power (~0.3 mW) at the sample. [K. F. Domke et al., J. Am. Chem. Soc. 128, 6708 (2007)]

*T*ip-*E*nhanced *R*aman *S*cattering (TERS)
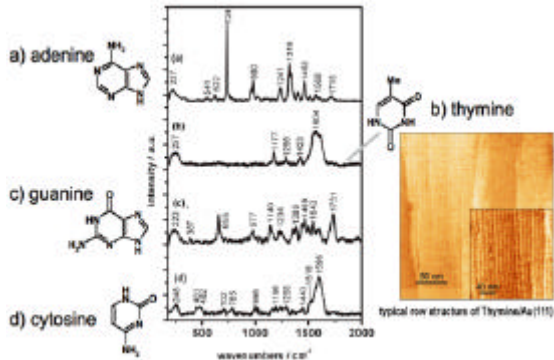
One monolayer of a DNA base (adenine, thymine, guanine or cytosine) is adsorbed on a Au(111) subtrate. When the **gold tip** is brought into tunneling contact, a strong enhancement of the Raman intensity is observed; if the tip is retracted, no Raman signal is detectable. The STM image on the right shows the typical row structure of the thymine monolayer. [K. F. Domke et al., J. Am. Chem. Soc. 128, 6708 (2007)]

Stimulated Raman scattering

Spontaneous Raman scattering is spatially isotropic, there is no correlation among emissions of different molecules.

Stimulated Raman scattering may occur when molecules are illuminated by two light beams at frequencies ω_p and ω_s, such that

$\omega_p - \omega_s = \omega_v$. One photon at frequency ω_p disappears, one photon at frequency ω_s is generated and the molecule goes into an excited vibrational state. The emission of the Stokes photon is directional and coherent, so that the beam at frequency ω_s is amplified.

Stimulated Raman scattering
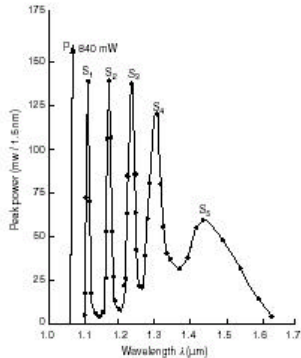
Generation of a sequence of Stokes lines by stimulated Raman scattering in a single-mode optical fiber by using a Nd laser as the optical source
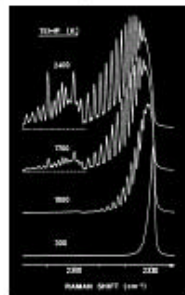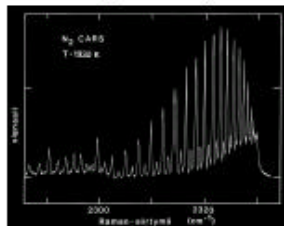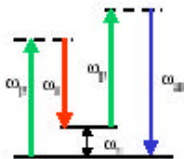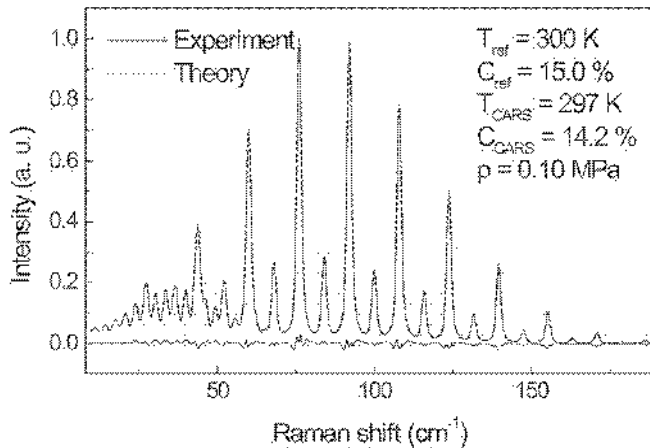
CARS

Coherent anti-Stokes Raman Scattering; CARS

Vibrational energy: $E_v = (v+1/2)h\nu_v$; Rotational energy: $E_r = r(r+1)h^2/(8\pi^2 I)$

# CARS in combustion diagnostics

Accumulated experimental spectrum (200 single shots) of a 15% CO2–N2 mixture 0.1 MPa; 300 K compared with the bestfitting theoretical spectrum. The difference of both spectra is depicted as well.[M. Schenk et al. Appl. Optics 44, 5582 (2005)]

CARS in combustion diagnostics
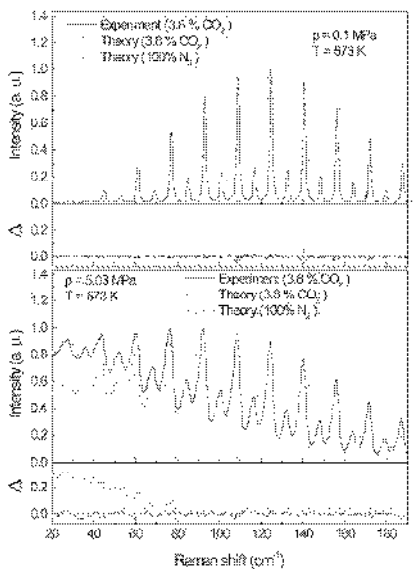
Increasing spectral influence of CO_2 relative to N_2 toward higher pressures. The figure displays the accumulated experimental spectra (3.8% CO2; 573 K at 0.1 and 5 MPa, top and bottom, respectively) compared with the best-fitting theoretical spectra of a 3.8% CO2 mixture with N2 as well as with the best-fitting theoretical spectra of pure N2. The corresponding difference spectra are depicted in the lower parts of both graphs.

CARS Endoscope
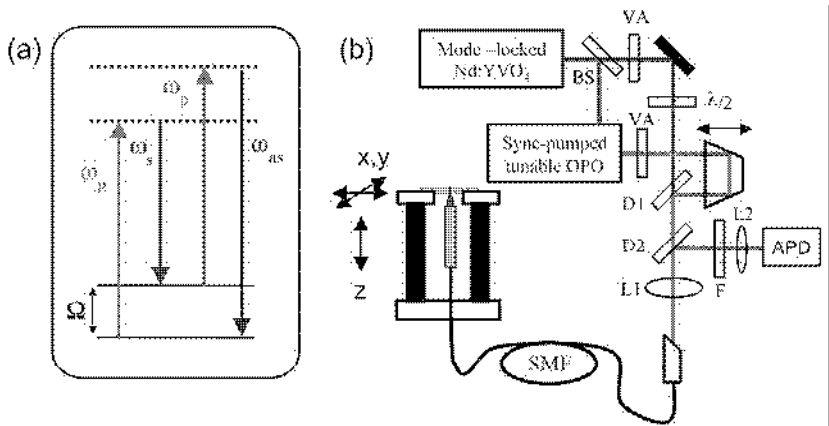
(a) CARS energy diagram. (b) Experimental setup: BS, 15% beam splitter; VA, variable attenuator; ?/2, half-waveplate; D1, 950nm longpass dichroic mirror; D2, 750nm longpass dichroic mirror; F, three 670nm bandpass filters; L1, aspheric lens; L2, 10cm concave lens.[F. Legaré et al. Opt. Express 14, 4427 (2006)]
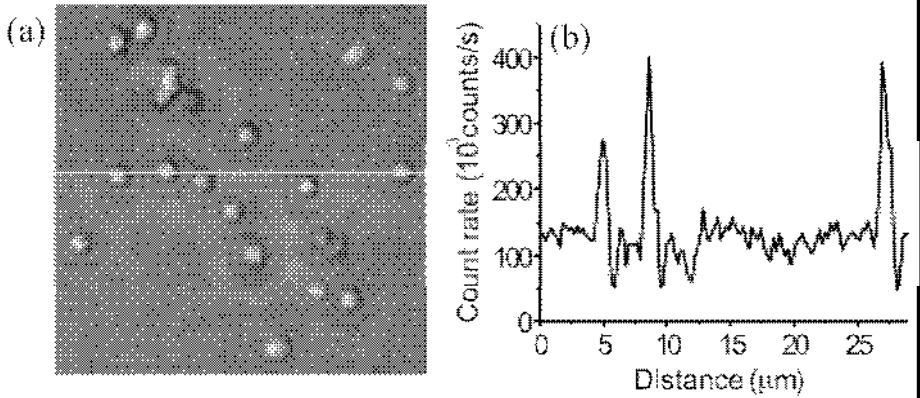
CARS Endoscope

An endoscope based on the vibrational contrast of CARS would offer label-free chemically-selective imaging *in situ*, making it an ideal tool for biomedical applications. In this report, we present a prototype CARS endoscope capable of imaging specimens with submicron lateral resolution and ~12 μm axial resolution.

The laser source consisted of a passively mode-locked 10W Nd:YVO$_4$ laser (High-Q Laser GmbH) operating at 1064 nm, which delivered transform-limited 7 ps pulses at a repetition rate of 76 MHz. The majority of the Nd:YVO$_4$ output (9 W) was used to synchronously pump an OPO (APE-Berlin). The OPO cavity was configured to resonate on its signal wavelength. and utilized intracavity-doubling to efficiently generate a 5ps pulse train with up to 2 W of average output power. A broad tuning range of 780-920 nm was achieved by adjusting the position and temperature of a multi-grating, periodically poled lithium niobate crystal used for parametric generation. A portion of the 1064 nm output (1.5 W) was used as a Stokes beam while the tunable OPO output provided the pump beam.
We characterized the performance of the prototype CARS endoscope by imaging size calibrated polystyrene beads with the pump and Stokes difference frequency set to the aliphatic symmetric CH$_2$ stretch (?? = 2845 cm^{-1}).

CARS endoscope

(a) Prototype CARS endoscope image of 0.75μm polystyrene beads embedded in agarose gel spin-coated on a coverslip (??=2845cm-1). The image dimension is 29μm×29μm (128×128 pixels). The pump and Stokes powers at the sample were 80mW each, with a pixel dwell time of 1ms. (b) CARS intensity profile along the white line in (a).

Multiphoton fluorescence
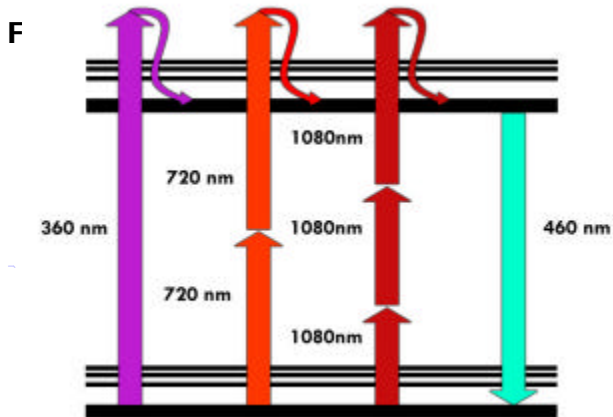
Perrin-Jablonski fluorescence diagram. Simplified Perrin-Jablonski scheme for 1PE, 2PE and 3PE. Once the excited state has been reached the subsequent fluorescent emission is the very same for the three different modalities of excitation.

Two-photon fluorophores

2PE excitation parameters.

| FLUOROPHORES	λ (nm)	ηd_2	d_2
Extrinsic fluorophores			
Bis-MSB	691/700	6.0 ± 1.8	6.3 ± 1.8
Bodipy	920	17 ± 4.9	-
Calcium Green	740–990	-	~80
Calcofluor	780/820	-	-
Cascade blue	750–800	2.1 ± 0.6	~3
Coumarin 307	776, 700–800	19 ± 5.5	~20
CY2	780/800	-	-
CY3	780	-	-
CY5	780/820	-	-

δ_2 is the absorption cross-section in units of 10^{-58} [$m^4 s$], η is the quantum efficiency

Confocal imaging
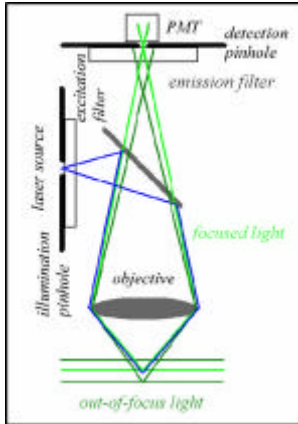
Confocal optical pathways. An illumination and a detection pinhole are placed in the optical pathway. The detection pinhole – the mask – is placed in front of the detector at a plane that is conjugate to the in-focus or "j" plane, such that the illumination spot and the pinhole aperture are simultaneously focused at the same specimen volume. This coincidence of the illumination and detected volume is responsible for confocality. The illumination pinhole allows to perform pointlike scanning.

Two-photon fluorescence
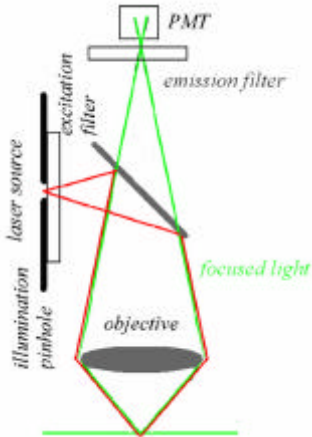
MPE simplified optical pathways. In the MPE optical pathways the emission pinhole is removed since the only emitted light reaching the sensor is coming from the currently point scanned volume in the sample. No other fluorescence signal is produced elsewhere.

Confocal fluorescence
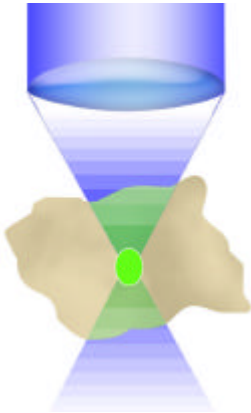
Confocal fluorescence emission distribution. The emission process, in green, under blue 1PE excitation is broadened in the whole double cone excitation shape within the analyzed cell.

Two-photon fluorescence
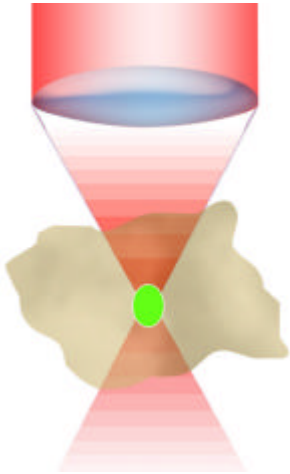
MPE fluorescence emission distribution. Confinement of the emission process, in green, under red 2PE. Under 2PE the only molecules excited are those confined in a small subfemtoliter volume at the illumination beam focus position. This is particularly relevant for the photobleaching process that is globally reduced with respect to the 1PE case. The capacity of the volume can be approximatively calculated by using the resolution parameters of the optical system, since they are indicators of the volume containing the maximum photon density. This is valid only for non saturated processes. Under saturation of fluorescence beam intensity plays an important role in the emission shape and optical resolution.

Two-photon fluorescence
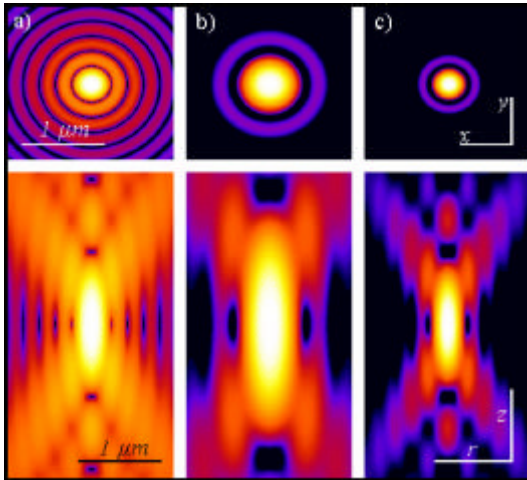

Pointlike emitter optical response. From left to right: calculated x-y (above) and r-z (below) intensity distributions, in logarithmic scale, for a point like source imaged by means of wide-field, 2PE and confocal microscopy. Both 2PE and confocal shapes exhibit a better signal to noise ratio than widefield case. 2PE distribution is larger due the fact that a wavelength twice than in the wide-field and confocal case is responsible for the intensity distribution. Such intensity distributions are also known as point spread functions of the related microscopes. Optical conditions: excitation wavelengths are 488 nm and 900 nm for 1PE and 2PE, respectively; emission wavelength is 520 nm; numerical aperture is 1.3 for an oil immersion objective with oil refractive index value set at 1.515.

Two-photon fluorescence
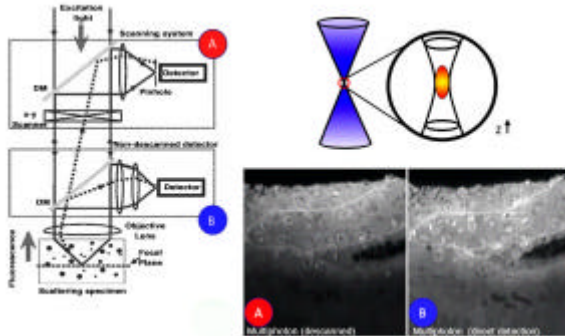
MPE simplified optical schemes. Descanned (red dot) and non-descanned (blue dot) schemes for 2PE microscopy. Due to the confinement of the excitation process when operating in non-descanned mode the collection efficiency in depth is increased as shown by the two side views from the very same thick scattering sample (Courtesy of Mark Cannel and Christian Soeller; image inset courtesy of Ammasi Periasamy).

Two-photon fluorescence
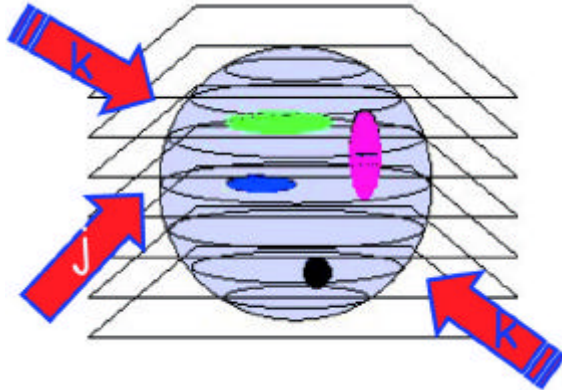
Optical sectioning scheme. A three-dimensional sample can be sketched as a series of optical slices. Let's call slice j the one containing the geometrical focus of the objective and refer to the adjacent planes as k slices. The sample contains a three-dimensional distribution of fluorescently labelled molecules whose intensity distribution is I, slice by slice. The thickness of each optical slice is approximately one half of the axial resolution, say ˜?/2.

Two-photon fluorescence

2PE and MPE microscopes are expected to increase their impact in areas such biotechnology, neurobiology, embryology, tissue engineering, materials science where imaging can be coupled to the possibility of using the microscopes in an active way, too. Clinically, 2PE may find applications in non-invasive optical bioscopy, while in cell biology the imaging abilities are coupled to the possibility of producing localized chemical reactions. Potential applications to integrative cardiac physiology or the possibility of tracking for long time biological events in living systems point out to the ability of making direct observations of phenomena and

circumstances that before could only be inferred using other approaches.

The great impact of 2PE in optical microscopy is related to the fact that it couples a three-dimensional intrinsic ability with almost five other interesting capabilities. First, 2PE greatly reduces photo-interactions and allows imaging of living specimens on long time periods. Second, it allows operating in a high-sensitivity background-free acquisition scheme. Third, 2PE microscopy can penetrate turbid and thick specimens down to a depth of a few hundreds micrometers. Fourth, due to the distinct character of the multiphoton absorption spectra of many of the fluorophores 2PE allows simultaneous excitation of different fluorescent molecules reducing colocalization errors. Fifth, 2PE can prime photochemical reactions within subfemtoliter volumes inside solutions, cells and tissues.

Two-photon fluorescence
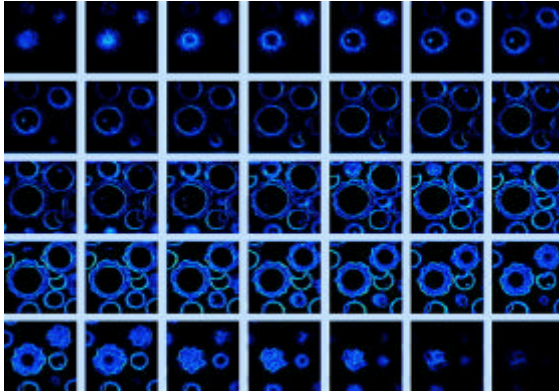
Optical sectioning using 2PE autofluorescence. 2PE optical sectioning of *Colpoda maupasi* resting cysts, 21–32 µm average dimensions. Encystment is particularly widespread in species living in ephemeral fresh-water puddles and is induced by exhaustion of the food and drying out. The resulting images have been obtained at LAMBS-MicroScoBio exploiting autofluorescence primed using 740 nm excitation. A Chameleon-XR ultrafast Ti-Sapphire laser (Coherent Inc., USA) and a Nikon PCM2000 confocal scanning head have been used [34]. Linear frame dimension is 70 µm, z steps have been performed every 0.5 µm, and not all the optical sections are imaged.

Two-photon fluorescence
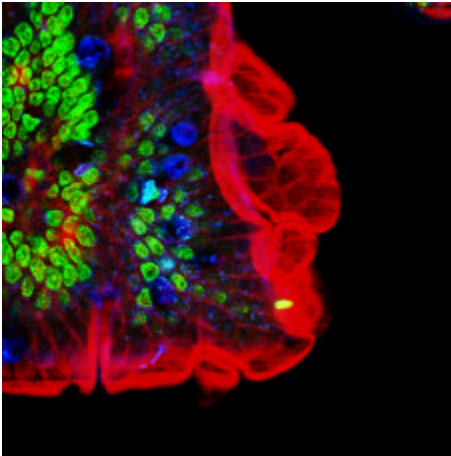
Multiple fluorescence 2PE imaging. 2PE multiple fluorescence image from a 16 µm cryostat section of mouse intestine stained with a combination of fluorescent stains (F-24631, Molecular Probes). Alexa Fluor 350 wheat germ agglutinin, a blue-fluorescent lectin, was used to stain the mucus of goblet cells. The filamentous actin prevalent in the brush border was stained with red-fluorescent Alexa Flu or 568 phalloidin. Finally, the nuclei were stained with SYTOX ® Green nucleic acid stain. Imaging has been performed at 780 nm, 100 x 1.4 NA Leica objective, using a Chameleon XR ultrafast Ti-Sapphire laser (Coherent Inc., USA) coupled at LAMBS-MicroScoBio with a Spectral Confocal Laser Scanning Microscope,

Leica SP2-AOBS.

Two-photon fluorescence
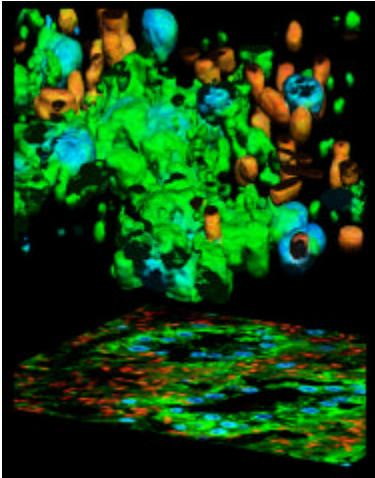
3D and 2D fluorescence projections. Pictorial representation of the 3D and 2D projections of multiple fluorescence from a marine sponge, *Chondrilla nucula*. The specimen has been loaded with Alexa 488 fluorescent molecules specific aminobutirric acid (GABA) emitting in green, DAPI for nuclear DNA for the blu component. Red signals are due to the autofluorescence from symbiontic bacteria contamination. Imaging has been perfomed using a Chameleon XR ultrafast Ti-Sapphire laser (Coherent Inc., USA) coupled at LAMBS-MicroScoBio with a Spectral Confocal L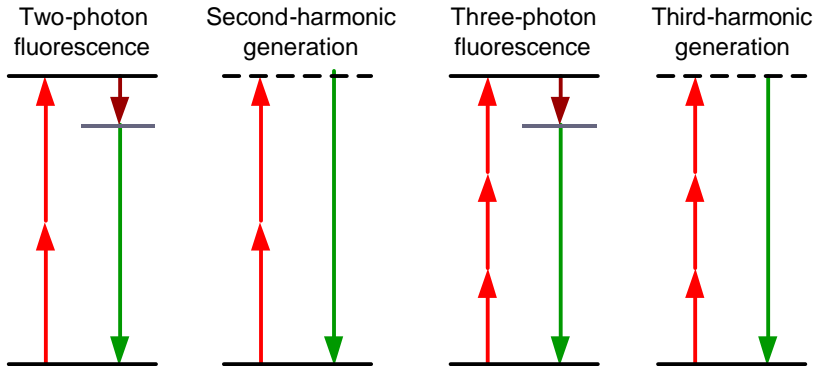aser Scanning Microscope, Leica SP2-AOBS. (Sample availability and preparation, courtesy of Renata Manconi, University of Sassari, Roberto Pronzato

and Lorenzo Gallus, University of Genoa).

NLO processes used in imaging

Two-photon fluorescence

Second-harmonic generation

Three-photon fluorescence

Third-harmonic generation

In third-order, one must use a longer wavelength laser (>1.0 μm) in order to avoid direct absorption of the third harmonic by the specimen.

Third-harmonic microscopy
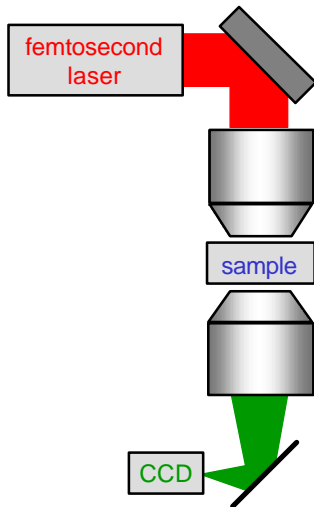
The third harmonic of the incident light is produced when an interface breaks the symmetry of the focus, providing inherent optical sectioning.

Normal optical microscope objectives are used to focus the input light and collect the TH

signal light.

The sample can be scanned in x

and y (and maybe z) directions.

This work has been pioneered by Squier and Muller, UCSD

THG imaging

In THG microscopy, third harmonic light is generated at the focal point of a tightly focused short-pulse laser beam. When the medium at the focal point is homogenous, the third harmonic waves generated before and after the focal point interfere destructively, resulting in zero net THG. However, when there are inhomogeneities near the focal point, such as an interface between two media, the symmetry along the optical axis breaks and measurable amount of third harmonic is generated. Due to its nonlinear nature, the third harmonic light is generated only in a close proximity to the focal point. Therefore, high lateral resolution can be obtained, allowing THG microscopy to perform sectioning and to construct three-dimensional images of transparent samples. Since all materials have non-vanishing third-order susceptibilities, THG microscopy can be utilized as a general-purpose microscopy technique.

D. Yelin and Y. Silberberg, Opt. Express 5, 169 (1999)

Characteristics of THG imaging

- Background-free imaging technique, requiring no additional staining.
- Provides inherent optical sectioning.
- Non-fading in nature (stains fade with time).
- Performed under same excitation intensities as 2-photon microscopy.
- Performed in transmission.
- Coherent imaging technique.
- Uses IR, rather than visible or UV, so is less damaging to the specimen.
- Is less bothered by phase distortions in the medium than conventional microscopy.

THG imaging apparatus

The laser source is a synchronously pumped OPO (Spectra-Physics Tsunami-Opal system) which provides 130 fs pulses at a wavelength of 1.5 μm at a repetition rate of 80 MHz. The laser beam is coupled through one of the microscope ports and is focused into the sample by the microscope objective. The focal point is scanned in the x-y plane using two optical scanners, and along the z-axis using the motorized stage of the microscope. The third harmonic light at the wavelength of 0.5 μm is collected by the original condenser (NA=0.63) and measured by a photomultiplier tube (PMT, Hamamatsu R4220) after filtering out the fundamental wavelength using a band-pass interference filter.

In the experiments reported below, the average laser power was 50 mW. Focusing the beam into an area of 1 μm^2, using the strongest microscope objective (NA=1.4oil) results in a peak intensity of 0.5 TW/cm^2, which is still below the threshold for ionization of atoms or molecules. When the focused beam is illuminating a single point for a few seconds, local heating often damages the sample. However, we have verified that scanning the sample at high rates eliminates this problem. Images composed of 300x300 pixels were taken in 30 seconds, i.e. only 0.3 ms per pixel.

Detection of "low contrast" interfaces

Demonstration using an optical fiber in index-matching fluid.

125 μm
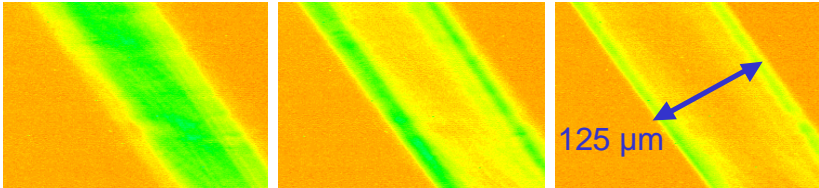
The third harmonic signal is generated at the interface of jacket and cladding; no image processing or background subtraction was used here. (~100 fs pulses at 1.2 μm, 1 kHz repetition rate.)

Images due to Jeff Squier, Colorado School of Mines

Orientation dependence of THG imaging
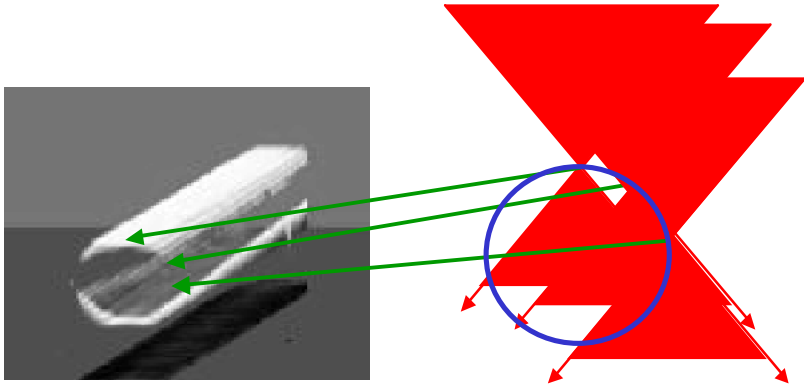
The different images show the fiber along different paths.

Sectional THG images of spiral algae formation
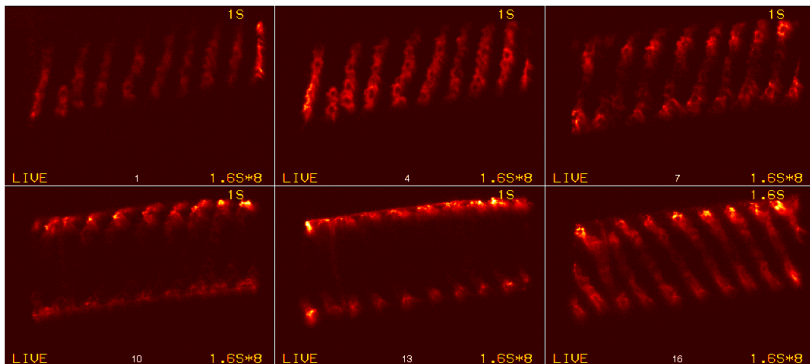
Excitation pulse: 100 fs, at 1.2 μm, at 250 kHz repetition rate.
~1.2 mW average power at sample.
Excitation objective: 20x, 0.6 NA Zeiss Plan-Apochromat
Collection objective: 20x, 0.4 NA Olympus
Cursor: single point, rastered in a traveling Lissajou pattern.
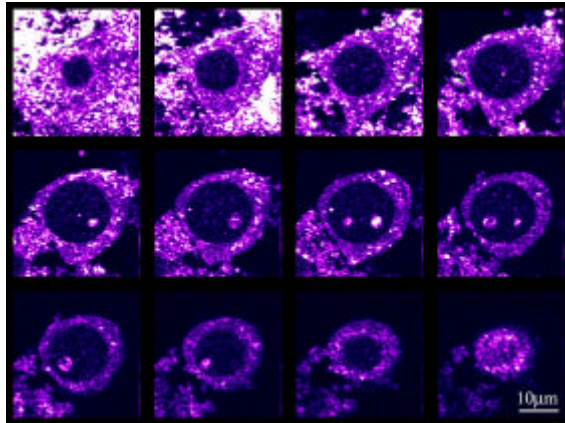Dispersion: ~500 fs^2, which results in ~30% pulse broadening.

3D reconstruction of spiral algae

The THG images of the previous slide allow this reconstruction.

Images due to Jeff Squier, Colorado School of Mines
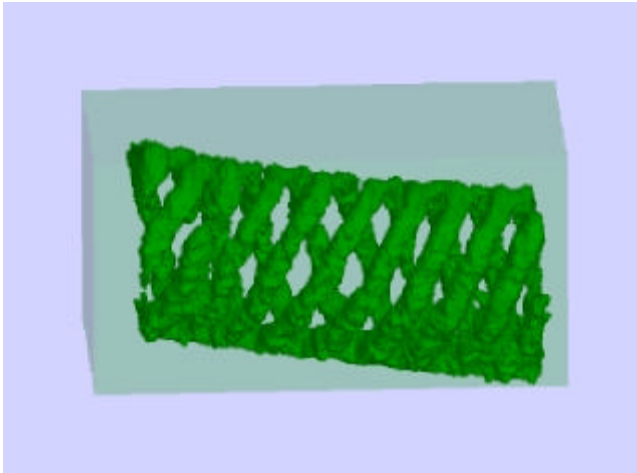
3D reconstruction of a live neuron

Sections of a live neuron. Each image is a horizontal section of the neuron's soma. The sections are separated by 0.5 μm. Two bright nucleoli are visible inside the dark nucleus.

Images due to Jeff Squier, Colorado School of Mines